Mechanochemical Sensing Devices

DOI: 10.1002/anie.201404043

Single-Molecule Mechanochemical Sensing Using DNA Origami Nanostructures**

Deepak Koirala, Prakash Shrestha, Tomoko Emura, Kumi Hidaka, Shankar Mandal, Masayuki Endo, Hiroshi Sugiyama,* and Hanbin Mao**

Abstract: *While single-molecule sensing offers the ultimate detection limit, its throughput is often restricted as sensing events are carried out one at a time in most cases. 2D and 3D DNA origami nanostructures are used as expanded single-molecule platforms in a new mechanochemical sensing strategy. As a proof of concept, six sensing probes are incorporated in a 7-tile DNA origami nanoassembly, wherein binding of a target molecule to any of these probes leads to mechanochemical rearrangement of the origami nanostructure, which is monitored in real time by optical tweezers. Using these platforms, 10 pM platelet-derived growth factor (PDGF) are detected within 10 minutes, while demonstrating multiplex sensing of the PDGF and a target DNA in the same solution. By tapping into the rapid development of versatile DNA origami nanostructures, this mechanochemical platform is anticipated to offer a long sought solution for single-molecule sensing with improved throughput.*

Mechanochemistry is an emerging discipline that investigates the coupling between mechanical and chemical processes.[1] Under mechanical stress, the stability of covalent or non-covalent interactions changes, which either strengthens or weakens molecular structures.[2] When a ligand binds to a receptor, the binding affinity between the receptor–ligand complex changes mechanical tension of either the free receptor or the ligand.[3] In mechanochemical sensing, such variation in mechanical signals is monitored.[4] Compared to fluorescence signals that are subject to numerous background noises, mechanical signals, such as tension in a molecule, experience little environmental interference. As a result, the signal-to-noise ratio is high in mechanochemical sensing. Since ligand binding is directly coupled to the change in the mechanical signal, target recognition and signal transduction units in a traditional sensor can be integrated, which improves the performance of the sensor by eliminating the noise originating from the extra components in conventional sensing strategies.

Because of the superior force and spatial resolutions, we have previously used optical tweezers to investigate the mechanochemical coupling in individual DNA or RNA molecules under various conditions.[5] However, the throughput of the method is low as only one sensing event can be monitored at a time. To increase the throughput, here we used the DNA origami nanostructures as sensing templates. Discovered by Rothemund in 2006,[6] DNA origami has been exploited to fabricate a wide range of 2D and 3D DNA nanostructures.[6,7] Such nanostructures have been extensively used in many applications including nanorobotics, molecular computation, drug delivery, and high-resolution spatiotemporal measurements.[8] However, the biosensing has not been explored well in DNA origami nanostructures.[9] Compared to inorganic-material-based substrates for biosensing, DNA origami structures provide a biocompatible environment. In addition, the chemical components of an origami nanostructure can be precisely controlled at any location in a modular fashion, which allows facile modification and convenient incorporation of many functional components in a 2D or 3D DNA origami without redesigning the whole nanoassembly from scratch.

As a proof of concept, we designed a 7-tile DNA origami nanostructure in which the recognition elements are placed in the interlocks that connect adjacent tiles (Figure 1a). The binding of a target to any of the recognition elements breaks the lock, which generates a change in mechanical signal. We used a PDGF aptamer[8e,10] as the first recognition element in each of the six interlocks. In the second example, we used the PDGF aptamer and a toehold DNA strategy[11] for multiplex sensing of the PDGF and a target DNA in a mixture. We anticipate that the DNA origami sensing described here will provide a new paradigm for high-throughput mechanochemical sensing at the single-molecule level.

To prepare a DNA origami structure, a single-stranded DNA scaffold can be folded into a predesigned 2D or 3D DNA nanostructure with the aid of DNA staples.[6] Using this strategy, we designed and synthesized a 2D DNA origami

[*] Dr. D. Koirala, P. Shrestha, S. Mandal, Prof. Dr. H. Mao
Department of Chemistry & Biochemistry and
School of Biomedical Sciences, Kent State University
Kent, OH 44240 (USA)
E-mail: hmao@kent.edu

T. Emura, Prof. Dr. H. Sugiyama
Department of Chemistry, Graduate School of Science
Kyoto University, Kitashirakawa-oiwakecho
Sakyo-ku, Kyoto 606-8502 (Japan)
E-mail: hs@kuchem.kyoto-u.ac.jp

K. Hidaka, Prof. Dr. M. Endo, Prof. Dr. H. Sugiyama
Institute for Integrated Cell Material Sciences (WPI-iCeMS)
Kyoto University, Kitashirakawa-oiwakecho
Yoshida-ushinomiyacho, Sakyo-ku, Kyoto 606-8501 (Japan)

Prof. Dr. M. Endo, Prof. Dr. H. Sugiyama
CREST (Japan) Science and Technology Corporation (JST)
Sanbancho, Chiyoda-ku, Tokyo 102-0075 (Japan)
E-mail: endo@kuchem.kyoto-u.ac.jp

[**] This research work was partially supported by the NSF (grant number CHE-1026532 to H.M.) and JST CREST and JSPS KAKENHI (grant numbers 24310097, 24104002, 25253004 to H.S. and M.E.).

Supporting information for this article is available on the WWW under http://dx.doi.org/10.1002/anie.201404043.

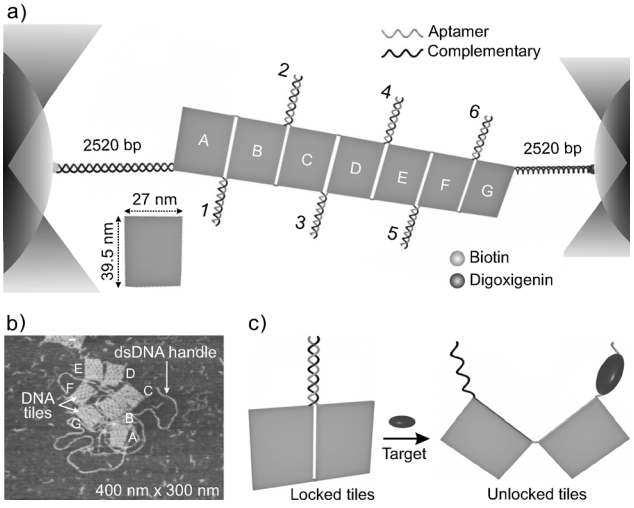

Figure 1. Mechanochemical sensing in optical tweezers using DNA origami nanostructures. a) Experimental setup (not to scale). A 7-tile 2D DNA origami nanoassembly is tethered between two optically trapped beads through dsDNA handles modified with a terminal digoxigenin or biotin. Each tile (marked A to G) of the origami has a dimension of 39.5×27 nm^2. The adjacent tiles are locked (marked 1 to 6) by an aptamer DNA (gray) and its complementary strand (black). b) AFM image (400×300 nm^2) of the origami nanoassembly depicting 7-tiles and two dsDNA handles. c) Illustration of the tile-unlocking due to the target binding to an aptamer lock. Binding of the target to the aptamer induces the folding of the aptamer, which releases the complementary strand and dissemble the lock.

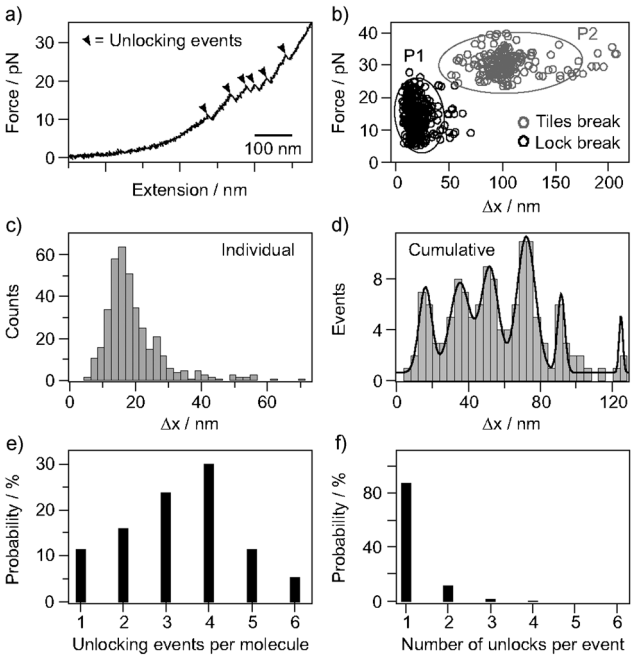

Figure 2. Mechanochemical properties of the 7-tile origami nanoassembly. a) A portion of a typical force–extension curve for the 7-tile nanoassembly, in which the aptamer lock is constituted by a PDGF aptamer and its complementary DNA strand (see Figure S5 for a complete *F–X* curve). The force-induced unlocking events are depicted by the arrowheads. b) The change in extension due to the unlocking (black circles) or tile disintegration (gray circles) events at a particular force (see text and SI for details). The ellipses represent 95% confidence interval for each population. c) Histogram of the change in extension for all individual cooperative events. d) Histogram of the cumulative change in extension of all events observed in single 7-tile nanostructures. e) Probability of unlocking in each nanoassembly shows that four unlocking events are most probable. f) Probability of cooperative unlocking events suggests that one-by-one, rather than simultaneous, unlocking is predominant.

comprising of seven interconnected tiles by using a linear M13mp18 DNA scaffold (Figure 1 a and b, see Table S1 in the Supporting Information for staple sequences and Figures S1 and S2 for additional AFM images). Each tile has a dimension of 39.5×27 nm^2. Two adjacent tiles are locked by using complementary DNA strands. One DNA strand contains an aptamer-based target recognition element that can change its conformation upon binding with a specific target,[8e,10] thereby unlocking the tiles (Figure 1 c). By attaching the terminal tiles of the DNA origami to the two optically trapped beads through dsDNA handles, the target binding and the unlocking events in the mechanochemical platform are monitored by optical tweezers (Figure 1 a).

Before sensing applications, we characterized the mechanical properties of this DNA origami construct. Although it is crucial to investigate mechanochemical properties of DNA nanostructures for material and biomedical applications, previously, only limited studies have been reported on the mechanical properties of rod-shaped DNA origami structures.[8h,12] We performed force-ramping experiments to increase the tension in the origami nanostructures by moving one of the traps away from the other. We observed two types of unfolding events in the force-extension curves. In the force range between 10–25 pN (Figure 2 a), we observed ≤ 6 events with a change-in-extension (Δx) of approximately 15 nm for each transition. This is consistent with the disassembly of the aptamer lock (Figure 2 b, black population P1). However, in the range above 30 pN (see Figure S5), we observed saw-teeth features with Δx of 100 nm (Figure 2 b, gray population P2). In a control construct without any interlocks between adjacent tiles, only ≥ 30 pN events were observed, confirming that the features between 10–25 pN are associated with the opening of the aptamer interlocks. Such an observation was further validated by performing experiments in which interlocks with shorter dsDNA were used. In these experiments, the unlocking forces were reduced, which reflects less Watson–Crick base pairing in the dsDNA lock. Based on these results, only the force range between 10–25 pN (Figure 2 b, black population P1) was considered for the mechanochemical sensing experiments.

The Δx histogram for all individual features of the P1 population shows a dominant peak at 15 nm with a shoulder at 25 nm (Figure 2 c). However, features with longer Δx were rare, suggesting unlocking events were non-cooperative. The cumulative Δx histogram (Figure 2 d) demonstrated six peaks with Gaussian centers of 14.0 ± 0.5, 33 ± 1, 50 ± 3, 70 ± 2, 90 ± 4, and 123 ± 4 nm, which were consistent with the predicted Δx patterns (see Table S2). The maximum probability of the peak at 70 nm indicates that 4 to 5 locks, instead of six, are most probable to be formed in an origami nanostructure. This was confirmed by the probability of the unlocked events per

molecule calculated from the observed Δx (Figure 2e, see Figure S6 for calculations). The observation of the four instead of six locks could be attributed to the incomplete assembly of the 7-tile DNA origami nanostructure itself or disassembly of the aptamer locks during the synthesis. The one-by-one, rather than simultaneous, unlocking of the tiles was confirmed in Figure 2f in which the most likely transitions were found to be associated with the single unlocking events.

After characterization of the unlocking in the 7-tile DNA origami, we employed this platform to detect the PDGF target. Binding of the PDGF to the aptamer strand in each lock helps to fold and stabilize the secondary structure of the aptamer,[8e,10] which leads to the disassembly of the origami tiles. Indeed, in the presence of 50 nM PDGF, unfolding of origami tiles was not observed as locks had been disintegrated by the binding of PDGF prior to the pulling experiments (Figure 3a). Analysis of the unlocking events per molecule confirmed this observation. Whereas a maximum of four unlocking events per molecule were observed without PDGF, zero unlocking was the most frequent observation with 50 nM PDGF (Figure 3b). To detect the binding of PDGF in real time, we switched the detection to the constant-force mode, in which the tension in the tethered molecule was maintained at 8 pN while the extension was monitored. As expected, the extension remained constant in a PDGF free solution over time (Figure 3c). With 25 nM PDGF, however, many extension-jumps were observed (Figure 3c). The size of each jump was consistent with expected values when neighboring tiles were separated (see Table S2). In addition, the patterns of the number of jumps were similar to that observed in the ramping-force mode in Figure 2e. Using the ramping-force and constant-force detection modes for high ($\geq$25 nM) and low ($\leq$0.1 nM) concentrations of the PDGF, respectively, we performed similar experiments in a range of PDGF concentrations. Figure 3d shows the probability of observing at least one unlocking event within 10 minutes. From this diagram, we estimated a detection limit of 10 pM (3σ) within 10 minutes. Compared to the detection limit of 100 pM in 30 minutes in a mechanochemical sensor that contains only one recognition element,[4] the results described here provide a strong support that the multiple recognition probes can effectively improve the detection by lowering the detection limit while significantly reducing the detection time.

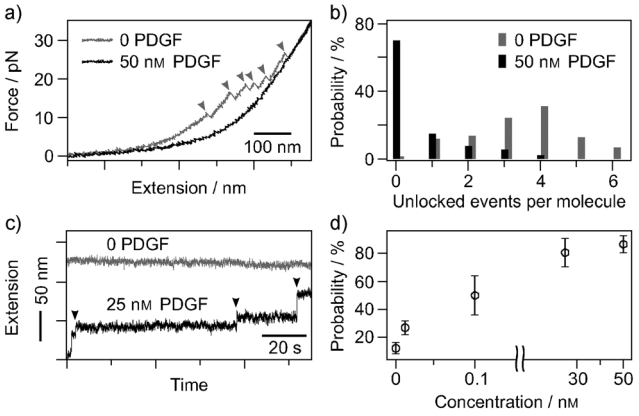

Figure 3. Mechanochemical sensing of PDGF using 7-tile nanoassembly in optical tweezers. a) Representative force-extension curves of the 7-tile DNA nanoassembly in the absence (gray) and presence (black) of 50 nM PDGF. In this ramping-force detection mode, the force-induced unlocking events (arrowheads) were absent in the solution containing the PDGF. b) Comparison of the unlocking events observed per molecule in the absence (gray) and presence (black) of the PDGF. The gray bars are slightly offset for clarity. c) Real-time observation of the target recognition events in the constant-force (8 pN) detection strategy. Without PDGF, no recognition events were observed. Upon switching to the target solution (25 nM PDGF), the binding of the target unlocked the tiles, leading to the extension jumps (arrowheads). d) The probability of detecting at least one unlocking event within 10 minutes as a function of PDGF concentration. Notice that below 0.1 nM, the constant-force detection strategy was used while ramping-force detection method was employed for higher concentrations.

Next, to demonstrate multiplexing capability of our mechanochemical sensing platform, we designed a DNA origami construct comprising of multiple recognition elements (Figure 4a). As a proof-of-concept, we incorporated two different probes in the two locks separately. One lock contains the same PDGF aptamer used above while the other consists of a DNA sequence (Oligo-B) to recognize its complementary DNA strand (Target DNA). Oligo-B contains a toehold segment in the toehold lock to preferentially bind to the target DNA over its partially complementary strand (Oligo-E; see the Supporting Information for DNA sequences). To well-differentiate the binding of each target, we placed the aptamer lock between tiles A and B; and the toehold lock, which comprises of Oligo-B and Oligo-E, between tiles B and E (see Figure 4a) All other tiles were left unconnected to reduce the complexity of the system. Such a design allows extension-jumps of 15 and 40 nm, respectively, for the recognitions of the PDGF by the aptamer lock and the Target DNA by the toehold lock (see Table S2 and Figure S7). Shown in the Figure 4b is an AFM image of a typical 7-tile DNA origami in which the connection between the tiles B and E is clearly shown due to the association between the Oligo-B and the Oligo-E (see Figure S3 for additional AFM images). In the presence of the Target DNA in the solution, the AFM images (see Figure S4) showed no such connections, indicating that the unlocking of these tiles is due to the target DNA binding.

With this design, we performed multiplex mechanochemical sensing using both ramping-force and constant-force detection modes in optical tweezers. During the ramping-force mode, the *F–X* curves showed two features in the target free buffer: one has Δx of 40 nm and other 15 nm (Figure 4c and d). These two values are consistent with the predicted Δx for the unlocking of the B-E and A-B tiles, respectively. In the presence of the target DNA (5 μM) that unlocks the B-E tiles by a toehold mechanism, only the 15 nm feature was observed in *F–X* curves (Figure 4e and f), which corresponded to the force-induced breaking of the A-B tiles. Similar results were obtained also in the presence of 500 nM target DNA. In the presence of the PDGF ligand that unlocks the A-B tiles, majority (80%) of the observed features were 40 nm (Figure 4g and h), which are associated with the mechanical unlocking of the B-E tiles. The 15 nm features were also observed in this case as a minor population (20%), suggesting

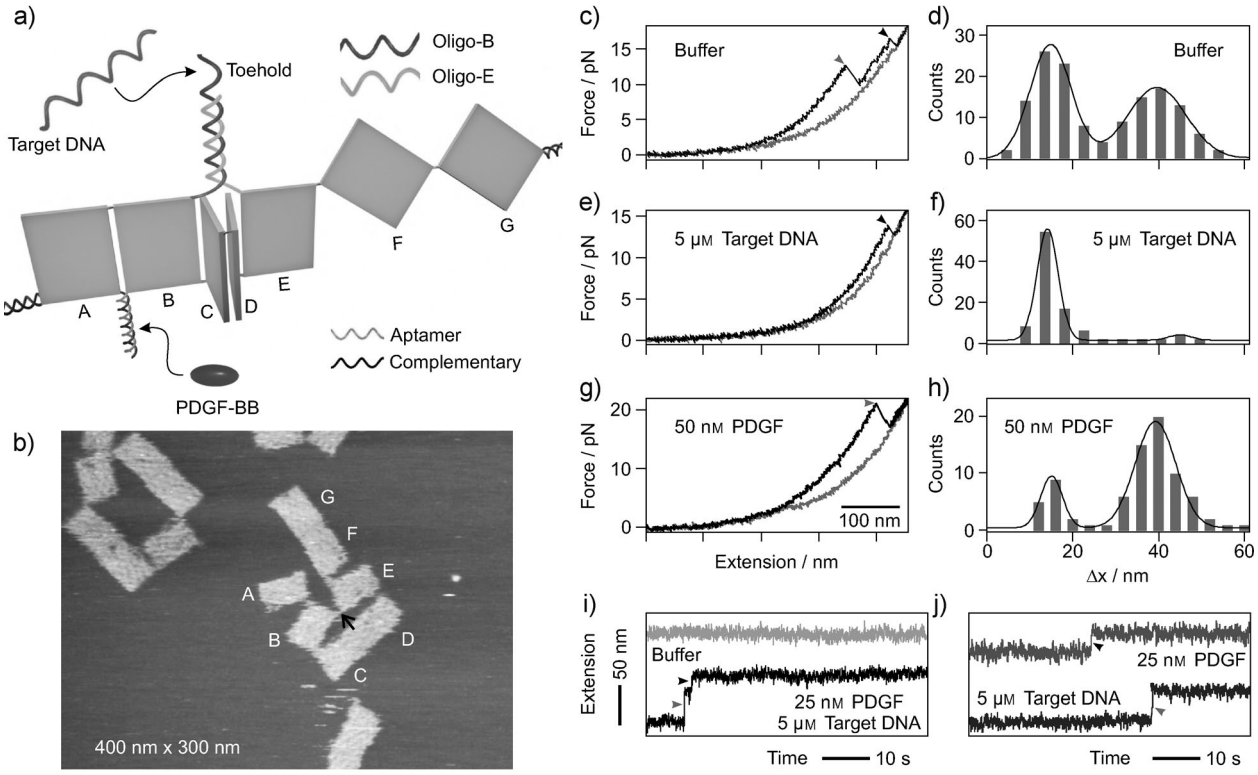

Figure 4. Simultaneous detection of multiple targets using a 3D origami nanoassembly. a) Schematic of the sensing platform. The lock between tiles A and B contains a PDGF aptamer sequence whereas that between the tiles B and E consists of a toehold DNA strand. All other tiles remain unlocked. b) An AFM image of the construct showing the connection (black arrow) between the tiles B and E. Note that this assembly does not contain the aptamer lock between tiles A and B. c,e,g) Typical force-extension curves. d,f,h) The corresponding Δx histograms. c,d) depict target free solution; e,f) depict 5 μM target DNA, and g,h) represent 50 nM PDGF. In target free solution, two force-induced unlocking events were observed. In the presence of one target, one unlocking event was observed. In the ramping-force detection mode, unlocking events were not observed in the presence of both targets (50 nM PDGF and 5 μM target DNA). i,j) Real-time detection of multiple targets in the constant-force mode (8 pN) at low concentrations (25 nM and 5 μM for PDGF and target DNA, respectively). In target free solution, the sensor showed no extension-jumps. i) When both targets were present, two extension-jumps consistent with the breaking of the two locks were observed. j) In the solution that contains only one target, one extension-jump was observed.

that a minor fraction of the locks between tiles A and B are not bound with PDGF. This observation is consistent with the slow binding kinetics between aptamer DNA and PDGF as reported in previous studies.[8e] Control experiments with non-target molecules, such as 100 ng μL^{-1} BSA, 5 μM scrambled DNA sequence, and 50 nM antidigoxigenin antibody, showed similar unlocking features as in target-free buffer, confirming the specificity of our mechanochemical sensing strategy (see Figure S8).

Further demonstration on the multiplex sensing came from experiments with the constant-force detection. When 8 pN was maintained in the origami template in the target free solution, breaking of the tiles was not observed (Figure 4i, upper trace). However, as soon as the sensor was taken to the solution mixture of 25 nM PDGF and 5 μM target DNA, two extension-jumps corresponding to the expected breaking of the two locks were observed (Figure 4i, lower trace). In the presence of individual targets, expected extension-jumps were observed for specific binding events (Figure 4j). These findings well established the capability of multiplex sensing in the DNA origami template. With the incorporation of more tiles and the full use of each tile, this mechanochemical sensing strategy is rather flexible to detect many different targets.

In summary, with a 7-tile DNA origami nanoassembly, we successfully demonstrated the principle of mechanochemical biosensing in optical tweezers. The incorporation of multiple recognition sites reduces the detection limit as well as the detection time. In addition, it offers a unique and versatile approach for multiplex biosensing. The mechanical signal with little background noise warrants a superior sensitivity of the sensor at the single-molecule level. With rapid development of DNA nanotechnology,[13] origami structures with increased mechanical stability and a wide range of target recognition sites are well within reach. We anticipate that the new sensing developed here will expand the applications of self-assembled DNA nanostructures into the mechanoanalytical chemistry, a new discipline that exploits mechanochemical principles for chemical analyses.

Received: April 6, 2014
Published online: June 16, 2014

Keywords: DNA nanotechnology · DNA origami nanostructures · mechanochemical sensing · optical tweezers · single-molecule techniques

[1] a) D. Keller, C. Bustamante, *Biophys. J.* **2000**, *78*, 541 – 556; b) A. L. Black, J. M. Lenhardt, S. L. Craig, *J. Mater. Chem.* **2011**, *21*, 1655 – 1663; c) H. T. Baytekin, B. Baytekin, B. A. Grzybowski, *Angew. Chem.* **2012**, *124*, 3656 – 3660; *Angew. Chem. Int. Ed.* **2012**, *51*, 3596 – 3600; d) P. A. May, J. S. Moore, *Chem. Soc. Rev.* **2013**, *42*, 7497 – 7506.

[2] a) M. K. Beyer, H. Clausen-Schaumann, *Chem. Rev.* **2005**, *105*, 2921 – 2948; b) C. Weder, *Nature* **2009**, *459*, 45 – 46; c) X. Zhang, K. Halvorsen, C.-Z. Zhang, W. P. Wong, T. A. Springer, *Science* **2009**, *324*, 1330 – 1334; d) L. Rognoni, J. Stigler, B. Pelz, J. Ylänne, M. Rief, *Proc. Natl. Acad. Sci. USA* **2012**, *109*, 19679 – 19684; e) S. L. Craig, *Nature* **2012**, *487*, 176 – 177; f) K. M. Wiggins, C. W. Bielawski, *Angew. Chem.* **2012**, *124*, 1672 – 1675; *Angew. Chem. Int. Ed.* **2012**, *51*, 1640 – 1643.

[3] a) D. Koirala, S. Dhakal, B. Ashbridge, Y. Sannohe, R. Rodriguez, H. Sugiyama, S. Balasubramanian, H. Mao, *Nat. Chem.* **2011**, *3*, 782 – 787; b) T.-H. Nguyen, L. J. Steinbock, H.-J. Butt, M. Helm, R. d. Berger, *J. Am. Chem. Soc.* **2011**, *133*, 2025 – 2027; c) P. M. Yangyuoru, S. Dhakal, Z. Yu, D. Koirala, S. M. Mwongela, H. Mao, *Anal. Chem.* **2012**, *84*, 5298 – 5303; d) D. Koirala, P. M. Yangyuoru, H. Mao, *Rev. Anal. Chem.* **2013**, *32*, 197 – 208.

[4] D. Koirala, Z. Yu, S. Dhakal, H. Mao, *J. Am. Chem. Soc.* **2011**, *133*, 9988 – 9991.

[5] a) Z. Yu, J. D. Schonhoft, S. Dhakal, R. Bajracharya, R. Hegde, S. Basu, H. Mao, *J. Am. Chem. Soc.* **2009**, *131*, 1876 – 1882; b) S. Dhakal, J. D. Schonhoft, D. Koirala, Z. Yu, S. Basu, H. Mao, *J. Am. Chem. Soc.* **2010**, *132*, 8991 – 8997; c) P. M. Yangyuoru, A. Y. Q. Zhang, Z. Shi, D. Koirala, S. Balasubramanian, H. Mao, *ChemBioChem* **2013**, *14*, 1931 – 1935; d) D. Koirala, J. A. Punnoose, P. Shrestha, H. Mao, *Angew. Chem.* **2014**, *126*, 3538 – 3542; *Angew. Chem. Int. Ed.* **2014**, *53*, 3470 – 3474.

[6] P. W. K. Rothemund, *Nature* **2006**, *440*, 297 – 302.

[7] a) S. M. Douglas, H. Dietz, T. Liedl, B. Högberg, F. Graf, W. M. Shih, *Nature* **2009**, *459*, 414 – 418; b) E. S. Andersen, M. Dong, M. M. Nielsen, K. Jahn, R. Subramani, W. Mamdouh, M. M. Golas, B. Sander, H. Stark, C. L. P. Oliveira, J. S. Pedersen, V. Birkedal, F. Besenbacher, K. V. Gothelf, J. Kjems, *Nature* **2009**, *459*, 73 – 76; c) A. Rajendran, M. Endo, Y. Katsuda, K. Hidaka, H. Sugiyama, *ACS Nano* **2010**, *5*, 665 – 671; d) D. Han, S. Pal, J. Nangreave, Z. Deng, Y. Liu, H. Yan, *Science* **2011**, *332*, 342 – 346.

[8] a) C. Mao, T. H. LaBean, J. H. Reif, N. C. Seeman, *Nature* **2000**, *407*, 493 – 496; b) N. L. Rosi, C. A. Mirkin, *Chem. Rev.* **2005**, *105*, 1547 – 1562; c) K. Lund, A. J. Manzo, N. Dabby, N. Michelotti, A. Johnson-Buck, J. Nangreave, S. Taylor, R. Pei, M. N. Stojanovic, N. G. Walter, E. Winfree, H. Yan, *Nature* **2010**, *465*, 206 – 210; d) A. V. Pinheiro, D. Han, W. M. Shih, H. Yan, *Nat. Nanotechnol.* **2011**, *6*, 763 – 772; e) S. M. Douglas, I. Bachelet, G. M. Church, *Science* **2012**, *335*, 831 – 834; f) A. Rajendran, M. Endo, H. Sugiyama, *Angew. Chem.* **2012**, *124*, 898 – 915; *Angew. Chem. Int. Ed.* **2012**, *51*, 874 – 890; g) H. Chandran, A. Rangnekar, G. Shetty, E. A. Schultes, J. H. Reif, T. H. LaBean, *Biotechnol. J.* **2013**, *8*, 221 – 227; h) E. Pfitzner, C. Wachauf, F. Kilchherr, B. Pelz, W. M. Shih, M. Rief, H. Dietz, *Angew. Chem.* **2013**, *125*, 7920 – 7925; *Angew. Chem. Int. Ed.* **2013**, *52*, 7766 – 7771.

[9] Y. Ke, S. Lindsay, Y. Chang, Y. Liu, H. Yan, *Science* **2008**, *319*, 180 – 183.

[10] L. S. Green, D. Jellinek, R. Jenison, A. Östman, C.-H. Heldin, N. Janjic, *Biochemistry* **1996**, *35*, 14413 – 14424.

[11] a) J. Fritz, M. K. Baller, H. P. Lang, H. Rothuizen, P. Vettiger, E. Meyer, H.-J. Güntherodt, C. Gerber, J. K. Gimzewski, *Science* **2000**, *288*, 316 – 318; b) J. J. Li, W. Tan, *Nano Lett.* **2002**, *2*, 315 – 318; c) D. Y. Zhang, A. J. Turberfield, B. Yurke, E. Winfree, *Science* **2007**, *318*, 1121 – 1125.

[12] D. J. Kauert, T. Kurth, T. Liedl, R. Seidel, *Nano Lett.* **2011**, *11*, 5558 – 5563.

[13] N. C. Seeman, *Nature* **2003**, *421*, 427 – 431.

